Experimental Eye Research 176 (2018) 174–187

Contents lists available at ScienceDirect

Experimental Eye Research

journal homepage: www.elsevier.com/locate/yexer

Retinal dysfunction parallels morphologic alterations and precede clinically detectable vascular alterations in *Meriones shawi*, a model of type 2 diabetes

Imane Hammoum[a,b], Maha Benlarbi[a], Ahmed Dellaa[a], Rim Kahloun[c], Riadh Messaoud[c], Soumaya Amara[c], Rached Azaiz[d], Ridha Charfeddine[d], Mohamed Dogui[e], Moncef Khairallah[c], Ákos Lukáts[f], Rafika Ben Chaouacha-Chekir[a,*]

[a] Laboratory of Physiopathology, Food and Biomolecules (PAB) of the High Institute of Biotechnology, Sidi Thabet (ISBST), Univ Manouba (UMA), BiotechPole Sidi Thabet, Tunisia
[b] Faculty of Sciences of Tunis, El Manar University (UTM), Tunis, Tunisia
[c] Service of Ophtalmology, Fattouma Bourguiba University Hospital, Monastir, Tunisia
[d] UNIMED Pharmaceutical Industry, Industrial Area Kalaa Kebira, Sousse, Tunisia
[e] Service of Functional Explorations of the Nervous System, Sahloul University Hospital, Sousse, Tunisia
[f] Department of Anatomy, Histology and Embryology, Semmelweis University, Budapest, Hungary

ARTICLE INFO

Keywords:
Type 2 diabetes
Ff-ERG
ISCEV
Meriones shawi
OCT
Fluorescein angiography

ABSTRACT

Diabetic retinopathy is a major cause of reduced visual acuity and acquired blindness. The aim of this work was to analyze functional and vascular changes in diabetic *Meriones shawi* (*M.sh*) an animal model of metabolic syndrome and type 2 diabetes. The animals were divided into four groups. Two groups were fed a high fat diet (HFD) for 3 and 7 months, two other groups served as age-matched controls. Retinal function was assessed using full field electroretinogram (Ff-ERG). Retinal thickness and vasculature were examined by optical coherence tomography, eye fundus and fluorescein angiography. Immunohistochemistry was used to examine key proteins of glutamate metabolism and synaptic transmission. Diabetic animals exhibited significantly delayed scotopic and photopic ERG responses and decreases in scotopic and photopic a- and b-wave amplitudes at both time points. Furthermore, a decrease of the amplitude of the flicker response and variable changes in the scotopic and photopic oscillatory potentials was reported. A significant decrease in retinal thickness was observed. No evident change in the visual streak area and no sign of vascular abnormality was present; however, some exudates in the periphery were visible in 7 months diabetic animals. Imunohistochemistry detected a decrease in the expression of glutamate synthetase, vesicular glutamate transporter 1 and synaptophysin proteins. Results indicate that a significant retinal dysfunction was present in the HFD induced diabetes involving both rod and cone pathways and this dysfunction correlate well with the morphological abnormalities reported previously. Furthermore, neurodegeneration and abnormalities in retinal function occur before vascular alterations would be detectable in diabetic *M.sh*.

1. Introduction

Diabetic retinopathy (DR) is a leading cause of blindness in adults (Congdon et al., 2003; Klein, 2007). The pathophysiology behind DR is complex: retinal vasculature and retinal neurons are both altered by the disease (Barber et al., 1998, 2000; Nguyen et al., 2007).

Clinically DR can only be easily diagnosed at the advanced stages based on the vascular abnormalities including microaneurysms, hemorrhages, cotton wool spots, hard exudates, intraretinal microvascular abnormalities, venous beading, loop formation and neovascularization (Gardner et al., 2002; Lai and Lo., 2013). Several techniques have been used for the detection, diagnosis and evaluation including eye fundus, fluorescein angiography and OCT (Salz and Witkin, 2015). While clinical diagnosis of DR focus on the visualization of retinal vascular lesions in diabetic patients, the disease also induces retinal electrophysiologic modifications including decreased contrast sensitivity, impaired color vision and ERG abnormalities (Ghirlanda et al., 1997; Greenstein et al., 1990; Hardy et al., 1992; Jackson and Barber, 2010). Indeed, these functional changes have been shown to occur in the retina prior to clinically detectable vascular symptoms (Juen and Kieselbach, 1990; Vadala et al., 2002; Yoshida et al., 1991) and may be the consequence of either the clinically undetectable microvascular pathology or the

* Corresponding author.
E-mail address: rafika.chekir@gmail.com (R. Ben Chaouacha-Chekir).

https://doi.org/10.1016/j.exer.2018.07.007
Received 27 March 2018; Received in revised form 19 June 2018; Accepted 5 July 2018

degeneration of glial and neural elements.

Much of the early disease progression seems to be similar between human patients and animal models; however, they never mimic exactly the human pathology (Wang et al., 2014). Consequently, choosing the right kind of animal model that is most representative of the structural, functional and biochemical features of human DR is of critical importance for investigating pathogenesis and for developing new and better therapeutic strategies. While rats and mice are the most commonly used animal models of DR, they have serious limitations including the different vasculature, the low cone number and the lack of fovea.

Meriones shawi (*M.sh*), a new animal model in DR researches, has the particularity to possess a prominent visual streak with outstandingly high cone and ganglion cell densities and specialized vasculature with the complete lack of major vessels in this area (Hammoum et al., 2017b). This anatomical composition resembling what can be seen in the human fovea makes this species a potentially useful model to mimic foveal pathology of DR including diabetic macular edema.

Furthermore, it's has been shown in our previous reports that feeding a high-fat diet (HFD) to *M.sh* for up to 3 and 7 months (Hammoum et al., 2017a, 2017b) caused evident retinal histological changes. In fact, we detected a significant decrease of retinal thickness, Müller glia activation with a significant increase in the number of microglia cells. In addition, prominent outer segment degeneration for both rods and cones, with a significant decrease in the number of all cones was visible. There was a decrease both in the staining intensity and in the number of stained elements for both AII and calretinin positive amacrine cells; furthermore, a significant loss of ganglion cells was also confirmed after 7 months in diabetic specimens.

The purpose of this study was to examine the clinical effects of HFD–induced diabetic conditions on retinal function and vasculature in *M.sh*, to evaluate how these changes progress with increasing diabetes duration and to correlate these changes with the previous results of the detailed histological evaluation. Special care was taken to examine the visual streak area in search for edema formation or any other specific pathological alterations. Additionally, we also aimed to extend the study to the key proteins of glutamate metabolism – the major neurotransmitter system of the retina - and synaptic transmission in general; as they have also been proposed to play important roles in the development of functional alterations and have not been examined in any previous report.

2. Material and methods

2.1. Experimental procedure

Approximately 3 months old male *M.sh* rodents (n = 40) were trapped in the semiarid region of Sidi Bouzid in BOUHEDMA Park (South of Tunisia), with the authorization of Tunisian Agriculture Ministry (number of approval: 2012–2016/2214-1693) and bred in our animal facility. All protocols on *M.sh* were approved by the ethics committee of Pasteur Institute, Tunis, Tunisia (number of approval: 2016/11/E/ISBST/V0). Animals were used and handled according to the principles of the Association for Research and Vision Research (ARVO) Statement for the Use of Animals in Ophthalmology and Vision Research.

Adult rodents, weighing 70–90 g were selected for the experiments. The animals were maintained at 24 ± 1 °C with 12/12 h light/dark photoperiod and free access to water and laboratory rodent chow.

After two weeks of adaptation period, the animals were divided into four groups. Two groups were fed a custom made high fat diet (Aissaoui et al., 2011) containing 14% protein, 60% complex carbohydrates, 10% sugar, 16% fat, 4% salt and 1% vitamin mix for an additional period of 3 months (n = 10) and 7 months (n = 10). The two other groups served as age-matched control animals maintained on standard laboratory diet containing only 4% fat (C3FG, El Badr company, Tunis, Tunisia) for 3 months (n = 10) and 7 months (n = 10). Water was supplied *ad libitum* to all groups. Body weights and blood glucose levels were monitored every month.

2.2. Clinical examinations

The examinations were performed at three months and seven months after HFD administration. Full field electroretinography (Ff-ERG), optical coherence tomography (OCT), eye fundus and fluorescein angiography (FA) were performed during the examinations.

2.2.1. Full field-Electroretinography

Retinal function was examined with Ff-ERG. Six responses were recorded with a Metrovision system (MonColor, Paris, France) according to the standardized protocol for clinical electroretinography by the International Society for Clinical Electrophysiology of Vision (ISCEV) and as it was already described in detail in our previous study (Dellaa et al., 2016). After 12 h of dark adaptation, animals were anesthetized under dim red illumination with ketamin (120 mg/kg, Tunisia) by intraperitoneal injection. Pupils were fully dilated with drops of tropicamide (25mg/5 ml; UNIMED, Sousse, Tunisia) and the animals were laid on a homeothermic blanket sets at 38 °C. The retinal potential was captured at the cornea with a low-mass, silver-coated, conductive (Dawson, Trick and Litzkow) fiber electrode (Sauquoit industries, Scranton, PA) acting as the active electrode. It was maintained on the cornea with an ophthalmic liquid gel lacryvisc (Carbomer 974 P, Alcon), to keep a proper conduction and to prevent corneal dryness. The reference and ground electrodes were inserted subcutaneously on the forehead and tail, respectively. The scotopic ERG responses (Amplification: x 12500; 1–1200 Hz bandwidth) were evoked to flashes of white light of 0.01 cd s m^{-2} for the rod response (RR) and 3 cd s m^{-2} for the mixed response (MR) and oscillatory potentials (OPs). The OPs were extracted from ERG signal using a 80–200 Hz bandwidth. After 10 min of light adaptation to a background of 30 cd m^{-2}, two photopic ERG responses (average, 20 flashes, inter stimulus interval: 1 s) were taken at 3 cd s.$m^{-2}$for the cone response (CR) and 30 Hz flicker response (FR).

2.2.2. Analysis of ERG parameters

Retinal function in diabetic and control animals was assessed by analyzing the amplitude and the latency of each waveform according to ISCEV protocol (Marmor et al., 2004; Zhang et al., 2014). The a-wave amplitude of the MR and CR was measured from the baseline to the first trough. The amplitude of the b-wave of the RR, MR and CR was measured from the first trough to the first peak. The amplitudes of scotopic and photopic OPs (OP1; OP2; OP3; OP4) and 30 Hz-Flicker response were measured from the through to the peak of each response component. The scotopic and photopic sum of the amplitudes of the OPs (ΣOPs = OP1 + OP2 + OP3 + OP4) was measured by adding the amplitudes of each of the sub-waves. The latency for all response peaks was calculated from stimulus onset to peak amplitude.

2.2.3. Optical coherence tomography

The pupils of animals were dilated as described above. Retinal imaging was performed using 3D OCT-2000 series (Topcon, Tokyo, Japan) with the integrated fundus camera. The average of the total retinal thickness measured from the nerve fiber layer to the outer margin of photoreceptor outer segments was calculated in diabetic and control *M.sh* from OCT-images by the FastMap software (Tokyo, Japan).

2.2.4. Eye fundus and fluorescein angiography

Fundus photography was taken as described previously (Huber et al., 2010; Paques et al., 2007; Xu et al., 2008). FA was performed by an intraperitoneal injection of fluorescein dye. To record FA, the device (Topcon medical systems TRC-50DX, Oakland, NJ) was operated in the fluorescence mode with the excitation light provided by a 488-nm

Argon laser. Images of diabetic and control animals were collected from the Topcon's IMAGEneti-base and selected for the analysis. Fundus of the retinal periphery of 7 months diabetic animals were taken by the integrated fundus camera of the OCT and isodensity maps of retinal thickness in the altered areas were given automatically by the FastMap software.

2.3. Immunohistochemistry

Immunohistochemistry was performed as described in our previous reports (Hammoum et al., 2017a, 2017b). In brief, at the end of the observation period, after all clinical examinations were performed; the animals were euthanized with the intraperitoneal injection of ketamin (120 mg/kg). Eyes were oriented, enucleated and fixed in 4% paraformaldehyde diluted in 0.1 M phosphate buffer (PB, pH 7.4), for 2 h at room temperature (RT) and then dissected. The remaining eyecups were cryoprotected in 30% sucrose diluted in PB overnight at 4 °C and were embedded in tissue-embedding medium (Shandon Cryomatrix, Thermo Scientific, UK) Vertically oriented radial sections (15 µm) were prepared and mounted on the surface of gelatin-coated slides.

Sections were pretreated with blocking solution (1% bovine serum albumin diluted in 0.1M phosphate buffered saline, containing 0.4% Triton-X100 (Sigma-Aldrich Kft, Budapest, Hungary)) for 2 h. Retinas were incubated with a rabbit anti-glutamine synthetase (GS, 1/500, Cat# G2781, RRID: AB_259853, Sigma Aldrich, Paris, France), rabbit anti-vesicular glutamate transporter-1 (VGluT-1, 1/1000, Cat# ABN1647, Q62634, Merck millipore, France) and rabbit anti-synaptophysin 38 KDa (SVP38, 1/500, Cat# SAB4502906, RRID: AB_10746692, Sigma Aldrich, Paris, France) overnight at 4 °C. Bounding was detected with appropriate species-specific Alexa-conjugated secondary antibodies (Alexa-488 or Alexa-594, 1:200, 2 h, RT, Thermo Fisher Scientific, Waltham, MA). All sections were cover-slipped with fluoroshield with DAPI (Sigma-Aldrich Kft, Budapest, Hungary).

2.4. Antibody characterization

The three antibodies used in this study (GS, VGluT-1 and SVP38) are commercially available and were produced by international companies. The monoclonal GS antibody, purchased from Sigma Aldrich (Paris, France), is a synthetic peptide corresponding to the C-terminal region of mouse GS (amino acids 357–373, this sequence is identical in human, bovine, rat, hamster and pig). Staining pattern in *M.sh* was identical to those observed in rats and *Psammomys* obesus (Riepe and Norenburg, 1977; Saidi et al., 2011a; 2011b), and showed the characteristic morphological features expected of Müller glial cells.

The immunogen of the polyclonal VGluT-1 was a Keyhole limpet hemocyanin conjugated peptide corresponding to 14 amino acids from the C-terminal region of rat VGluT-1. Its specificity was tested by immunohistochemistry in rats, mice and human (Johnson et al., 2003; Sherry et al., 2003). The staining pattern in *M.sh* was identical, localized exclusively to the outer and inner plexiform layers.

The polyclonal SVP38 antibody was raised against a synthesized peptide derived from human synaptophysin. The reactivity was tested by immunohistochemistry in human, rats and mice (Dan et al., 2008; Nag and Wadhwa, 2001). In *M.sh*, an identical staining pattern was observed, localized specifically in the outer and inner plexiform layers of the retina.

2.5. Image capture and quantification of immunohistochemistry

Retinas were examined with a Zeiss LSM 780 Confocal System coupled to a Zeiss Axio Imager upright microscope. Stack images were recorded using Zen 2012 software (Carl Zeiss, Oberkochen, Germany) using strictly identical settings for the control and diabetic retinas. Representative images were created and the quantification of staining intensity were performed using FIJI (Schindelin et al., 2012). Adjacent layers from 5 µm retinal thickness were merged (5 layers) using maximum intensity projection and the fluorescent staining intensity was quantified in the inner plexiform layer (IPL) in case of VGluT-1 and SVP38 and the complete retina (from the inner to the outer limiting membranes) for GS. The thickness of the counting frame was 18 µm during all measurements and the height was adjusted to IPL or whole retinal thickness.

2.6. Statistics

Values are given as mean ± standard error (SE). Unpaired *t*-test was performed with the GRAPHPAD Prism 6 program (GraphPad Software Inc., La Jolla, CA) to calculate differences between diabetic groups and age-matched controls. P values less than or equal to 0.05 were considered statistically significant.

3. Results

3.1. Body weight and blood sugar levels in Meriones shawi

Results of body weight and blood sugar parameters were interpreted in details in our previous reports (Hammoum et al., 2017a, 2017b). There was no significant difference in body weights and blood glucose levels between the groups at the start of the experiment (baseline values). HFD induced a significant increase of body weight in diabetic animals compared to controls both after 3 months and 7 months. In Parallel, blood sugar levels also increased significantly in diabetic animals at both timepoints. The main parameters of the animal groups and the p values are summarized in Table 1.

3.2. Diabetes induces scotopic ERG abnormalities in Meriones shawi

Under scotopic conditions, two different responses were recorded. At lower light intensity (0.01 cd s m^{-2}), the retinal light response was mainly rod-pathway driven (Fig. 1a and b), while at the higher light intensity (3 cd s m^{-2}), the retinal light response was a mixture from rods and cones (Fig. 1c and d). Details of the statistical analysis with the appropriate p values are summarized in Table 2.

In the RR, we observed a significant decrease in the amplitude of the b-wave (Table 2) in diabetic animals compared to controls which was −27.99% at the stage of 3 months and −45.58% at 7 months of diabetes. The implicit time of the b-wave (Table 2) was also affected by diabetes both after 3 and 7 months.

MR analysis showed a significant reduction in the amplitude of the a-wave (Table 2) which was −33.4% after 3 months and −43.23% after 7 months of diabetes. No delay in the implicit time of the a-wave

Table 1
Body weight and blood sugar measurements.

Parmeters	Control 3 m		Diabetic 3 m		Control 7 m		Diabetic 7 m	
Period	Baseline	3 m	Baseline	3 m	Baseline	7 m	Baseline	7 m
Weight (g)	73.11 ± 1.91	78.8 ± 1.51	74.43 ± 2.43	157.93 ± 1.78****	75 ± 1.48	82.79 ± 1.12	78.25 ± 2.39	258.95 ± 3.32****
Blood sugar (mmol/l)	4.56 ± 0.14	4.42 ± 0.09	4.44 ± 0.09	10.24 ± 0.27****	4.33 ± 0.11	4.61 ± 0.10	4.44 ± 0.12	11.76 ± 0.39****

****p < 0.0001.

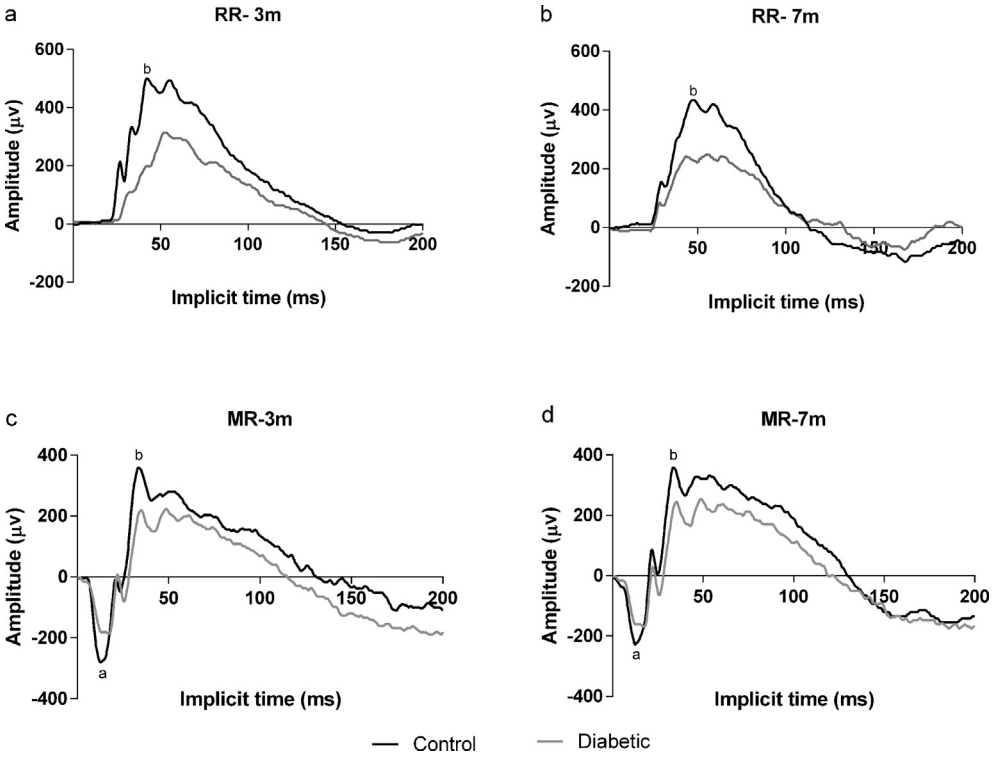

Fig. 1. Diabetes induces abnormal scotopic response in *Meriones shawi*. Representative rod responses (RR) stimulated using 0.01 cd s m^{-2} intensity and representative mixed (MR) responses using 3 cd s m^{-2} in control and diabetic *M.sh* at 3 months (3 m) (a-c) and 7 months (7 m) (b-d). Amplitude and implicit time of the RR b-wave showed a significant decrease at both 3 and 7 months of diabetes. The amplitudes of both MR a- and b-waves showed a significant decrease in 3 and 7 months diabetic animals. A delay in the implicit time was also noticed for the b-wave after both 3 and 7 months of diabetes but not for the a-wave at any point examined.

(Table 2) was noticed in diabetic animals. For the b-wave, a significant decrease in the amplitude (Table 2) was detected in diabetic animals compared to their age-matched controls, which was −24.64% at 3 months and −38.87% at 7 months of diabetes. The implicit time of the b-wave (Table 2) was also altered after both 3 and 7 months of diabetes.

Further analysis of scotopic b/a-wave ratio (Table 2) did not reveal any modifications in diabetes.

3.3. Diabetes induces photopic ERG abnormalities in Meriones shawi

In photopic conditions, the retinal responses were mainly cone driven. Two different responses were taken after light adaptation, at an intensity of 3 cd s m^{-2} for the CR (Fig. 2a and b) and the 30 Hz FR (Fig. 2c and d). Details of the statistical analysis are listed in Table 1.

Diabetes led to a significant reduction in the amplitude of the CR a-wave (Table 2) which was −55.47% and −63.62% in 3 months and in 7 months diabetic animals respectively compared to their age-matched controls. The implicit time of the a-wave (Table 2) was altered only after 7 months of diabetes induction in the treated group. Similarly to the RR and MR, a significant reduction in the amplitude of the b-wave (Table 2) was observed in diabetic animals compared to controls at 3 months (−41.04%) and at 7 months (−43.92%). We also observed that the b-wave implicit time (Table 2) was significantly affected in diabetic animals at the third and seventh month.

No significant change was noticed in the photopic b/a-wave ratio (Table 2) neither after 3 months nor after 7 months of diabetes.

The amplitude of the 30 Hz FR (Table 2) was also affected by diabetes starting from the third month with a reduction of −38.87%. At the end of the experiment, in 7 months diabetic animals an even greater decrease of −62.57% was detectable. No difference in the implicit time was observed in the two diabetic groups compared to their age-matched controls (Table 1).

3.4. Diabetes induces scotopic and photopic oscillatory potential abnormalities in Meriones shawi

The analysis of scotopic OPs (Fig. 3a and b) showed a significant decrease in the amplitude of OP2 (−31.87%), OP3 (−31.41%), OP4 (−29.7%) and ΣOPs (−29.22%) in 3 months diabetic animals. Delays in the implicit time were also noticed for OP2 and OP3 after 3 months of diabetes (Table 2). In the 7 months diabetic group, a more significant reduction in the amplitude of OP2 (−32%), OP3 (−42.47%), OP4 (−37.47%) and ΣOPs (−32.93%) was observed (Table 2). Similarly to the 3 months group, a delay of the implicit time of OP2 and OP3 was detected at this stage.

All the four photopic OPs (Fig. 3c and d) were altered already in the third month of diabetes and even more significantly in the seventh month. In 3 months diabetic animals, the decrease of the amplitude was −64.17% for OP1, -51.13% for OP2, -48.04% for OP3, -47.19 for OP4 and -51.09% for ΣPOs. At the end of the seventh month, this reduction increased to −73.5% for OP1, -73.85% for OP2, -65.68% for OP3, -66.37% for OP4 and -69.21% for ΣOPs. The implicit time was also delayed after 3 months for OP1, OP2 and OP3 and after 7 months for OP3 and OP4.

3.5. Diabetes induces a decrease in retinal thickness in Meriones shawi

OCT measurements (Fig. 4a–e) showed a significant decrease in total retinal thickness in diabetic (D) *M.sh* both after 3 months (C: 186.08 ± 4.54 µm, D: 155.65 ± 7.86 µm, $p = 0.021$) and after 7 months (C: 191.76 ± 5.77 µm, D: 143.11 ± 1.86 µm, $p = 0.002$) in comparison to their age-matched controls (C).

3.6. Assessment of retinal vasculature in diabetic Meriones shawi

The retinal vasculature of *M.sh* was extensively examined in two regions specifically by eye fundus and fluorescein angiography: the optic nerve and the macula-like zone (visual streak) (Fig. 5). Fundus images and fluorescein angiographs did not show any vascular abnormalities neither after 3 months nor after 7 months compared to their age matched controls. No evidence of any alteration resembling macular edema was observed in the visual streak area in the superior part of the retina in diabetic animals. In addition, no sign of ischaemia, neovascularization or fluorescein dye leakage was noticed. However,

Table 2
Amplitudes and implicit times of scotopic and photopic ERG responses in *Meriones shawi*.

ERG parameters	Control (3 m)	Diabetic (3 m)	p-value	Control (7 m)	Diabetic (7 m)	p-value
b-wave (RR)						
Amplitude (μv)	440.6 ± 20.20	317.3 ± 15.53	*** 0.0002	391.4 ± 11.6	213 ± 15.34	**** < 0.0001
Latency (ms)	44.08 ± 1.22	49.94 ± 2.37	*0.046	48.62 ± 1.77	54.95 ± 2.09	*0.033
a-wave (MR)						
Amplitude	234.2 ± 11.90	156 ± 8.91	**** < 0.0001	232.5 ± 13.92	132 ± 8.69	**** < 0.0001
Latency	13.11 ± 0.61	14.43 ± 0.57	0.13	12.40 ± 0.37	13.47 ± 0.56	0.13
b-wave (MR)						
Amplitude	498.5 ± 22.35	375.7 ± 14.40	**** < 0.0001	491.2 ± 20.16	300.3 ± 12.34	***0.0003
Latency	38.42 ± 2.13	45.95 ± 2.37	*0.03	37.07 ± 1.53	45.95 ± 2.48	**0.0083
Ratio b/a	2.14 ± 0.06	2.45 ± 0.13	0.054	2.14 ± 0.10	2.35 ± 0.17	0.31
Scotopic OPs						
OP1 (amplitude)	116.7 ± 17.05	87.36 ± 11.24	0.16	109.3 ± 15.16	78.83 ± 12.28	0.13
OP2 (amplitude)	139.4 ± 17.65	94.98 ± 8.41	*0.042	141.4 ± 15.56	96.16 ± 14.62	*0.048
OP3 (amplitude)	55.54 ± 4.94	38.10 ± 4.48	*0.017	55.46 ± 7.57	31.91 ± 2.91	*0.013
OP4 (amplitude)	32.42 ± 1.91	22.90 ± 3.57	*0.035	33.10 ± 3.88	20.70 ± 2.37	*0.015
ΣOPs (amplitude)	343.7 ± 36.03	243.3 ± 14.67	*0.024	339.3 ± 32.09	227.6 ± 27.78	*0.017
OP1 (latency)	19.61 ± 0.92	19.08 ± 0.87	0.5	18.64 ± 1.14	18.80 ± 0.69	0.90
OP2 (latency)	25.79 ± 0.79	29.12 ± 1.04	*0.02	25.83 ± 1.13	29.9 ± 1.24	*0.02
OP3 (latency)	38.58 ± 1.28	42.07 ± 0.96	*0.044	36.68 ± 1.28	40.12 ± 0.62	*0.031
OP4 (latency)	50.08 ± 1.6	51.65 ± 1.18	0.44	50.10 ± 1.68	51.33 ± 0.82	0.52
a-wave (CR)						
Amplitude	16.57 ± 2.69	7.38 ± 0.69	** 0.0078	14.84 ± 1.79	5.4 ± 0.73	*** 0.0004
Latency	16.49 ± 0.55	17.10 ± 0.77	0.53	16.29 ± 0.45	19.27 ± 1.16	*0.034
b-wave (CR)						
Amplitude	152.4 ± 10.04	89.87 ± 6.40	**** < 0.0001	139.8 ± 10.87	78.40 ± 4.85	**** < 0.0001
Latency	47 ± 1.35	58.17 ± 3.91	*0.020	47.20 ± 1.60	68.52 ± 2.72	**** < 0.0001
Ratio b/a	11.61 ± 1.83	13.54 ± 1.90	0.47	10.91 ± 1.49	14.21 ± 2.19	0.23
30-Hz flicker (FR)						
Amplitude	56.97 ± 2.59	34.83 ± 0.75	**** < 0.0001	55.11 ± 2.64	20.63 ± 1.98	**** < 0.0001
Latency	34.49 ± 0.17	34.54 ± 0.22	0.85	34.23 ± 0.39	34.56 ± 0.32	0.53
Photopic OPs						
OP1 (amplitude)	7.9 ± 0.97	2.83 ± 0.45	***0.0004	10.3 ± 1.16	2.73 ± 0.52	**** < 0.0001
OP2 (amplitude)	10.23 ± 1.39	5 ± 0.63	**0.0049	12.12 ± 2.09	3.17 ± 0.18	** 0.002
OP3 (amplitude)	13.26 ± 2.59	6.89 ± 0.93	*0.041	15.53 ± 2.94	5.33 ± 0.83	** 0.0071
OP4 (amplitude)	15.81 ± 1.43	8.35 ± 1.6	**0.0028	15.37 ± 1.06	5.17 ± 0.76	**** < 0.0001
ΣOPs (amplitude)	47.20 ± 4.82	23.09 ± 2.68	***0.0006	53.32 ± 5.52	16.42 ± 1.48	**** < 0.0001
OP1 (latency)	14.74 ± 1.22	19.49 ± 1.37	* 0.019	15.68 ± 1.12	18.51 ± 1.06	0.083
OP2 (latency)	25.95 ± 1.54	30.46 ± 1.37	* 0.042	27.26 ± 1.42	29.21 ± 1.31	0.32
OP3 (latency)	37.35 ± 1.01	41 ± 1.04	*0.02	38.20 ± 0.81	41.95 ± 1.42	*0.037
OP4 (latency)	47.26 ± 1.2	49.83 ± 1.29	0.16	46.37 ± 0.82	49.97 ± 1.43	* 0.046

RR: rod response, MR: mixed response, CR: cone response, FR: flicker response, OP: oscillatory potential. *p < 0.05, **p < 0.01, ***p < 0.001, ****p < 0.0001.

after 7 months of diabetes, eye fundus images showed some lesions that could be exudates (Fig. 6) in the superior periphery of the retina, which was also observed on OCT images. Isodensity maps of the retinal thickness also demonstrate disproportional distribution in the altered regions in diabetic animals compared to controls.

3.7. Diabetes induces changes in glutamate metabolism and synapse formation in Meriones shawi

Glutamate is the major neurotransmitter system in the retina. Alterations in glutamate synthesis, uptake and synapse formation in general effect retinal function and the ERG responses, so the analysis was extended to these parameters as well.

In controls, GS immunoreactivity was found radially in the retina from the inner limiting membrane to the outer limiting membrane, the labeling was localized in the cell processes and perikarya of Müller cells – as in every other species studied so far (Riepe and Norenburg, 1977; Saidi et al., 2011a; 2011b). A decrease of GS staining intensity (Fig. 7k) was noticed in diabetic animals after 3 months (C: 37.14 ± 0.81, D: 15.99 ± 0.58, p < 0.0001) (Fig. 7a–b) that became more pronounced after 7 months (C: 32.90 ± 1.12, D: 15.31 ± 1.69, p < 0.0001) (Fig. 7d–e).

VGluT-1 was located in the glutamatergic nerve terminals in the outer and inner plexiform layers in *M.sh* rodents. After 3 months of diabetes, a significant decrease in the staining intensity was noticed in diabetic animals. The intensity values in the IPL (Fig. 7l) were 45.90 ± 0.63 in control vs. 25.77 ± 1.36 in diabetic animals after 3 months (p < 0.0001) (Fig. 7f–g) and 44.75 ± 1.24 in control vs. 18.33 ± 1.13 in diabetic animals after 7 months (p < 0.0001) (Fig. 7i–j).

SVP38 is a presynaptic marker showing strong immunolabeling in both plexiform layers similarly to VGluT-1 in control *Meriones shawi* (Fig. 8a,d). Diabetes induced a significant decrease of SVP38 expression (Fig. 8g) after 3 months (C: 50.32 ± 2.15, D: 27.96 ± 1.31, p < 0.0001) and 7 months (C: 46.96 ± 1.45, D: 20.40 ± 0.66, p < 0.0001) of diabetes (Fig. 8c,f).

4. Discussion

In previous reports, we have presented histopathologic data on the retina of *M. sh*, a new rodent model of metabolic syndrome and type 2 diabetes. A series of morphologic examinations showed alteration of photoreceptors as well as inner retinal cell types after two different duration of the disease. In the present study, we reexamined the model with clinically available and frequently used methods including ERG, OCT and fundoscopy to examine the impact of diabetic conditions on retinal function and vasculature and to match the data with the structural changes reported. Additionally, we also examined key proteins of glutamate metabolism and synaptic transmission by immunohistochemistry. These factors are known to affect retinal function and the ERG, but were not examined in our previous report.

In summary, we detected abnormalities in retinal function before

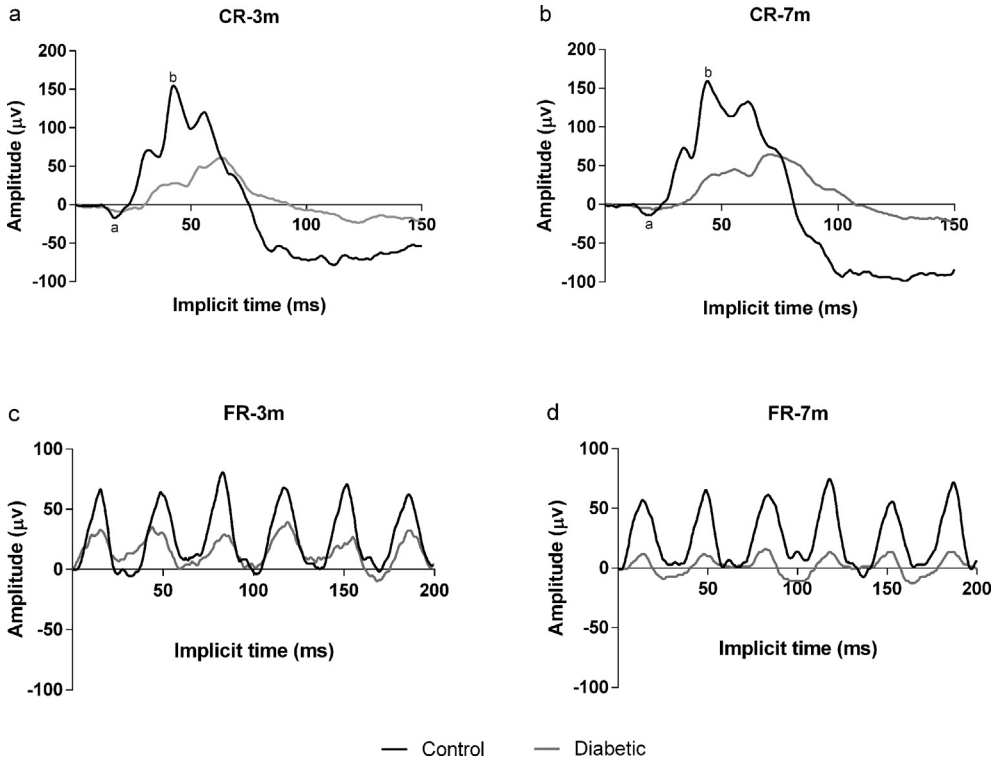

Fig. 2. Diabetes induces abnormal photopic response in *Meriones shawi*. Representative cone responses (CR) and 30 Hz-flicker responses (FR) stimulated using 3 cd s m^{-2} intensity in control and diabetic *M.sh* at 3 months (3 m) (a-c) and 7 months (7 m) (b-d). Diabetes induced a significant decrease in the amplitude of the a- and b-waves after both 3 and 7 months. A delay in the implicit time of the b-wave was detected at both time points in diabetic animals while for the a-wave only from the seventh month of diabetes. A significant decrease of the amplitude of the FR was detected after both 3 and 7 months of diabetes. No modifications were detectable in the implicit time in diabetic animals.

the onset of fundoscopically evident retinopathic changes. The functional abnormalities were similar to those reported by others in different animal models and human patients; and demonstrated evident correlation with structural alterations reported here and in our previous report. No edema formation was detectable in the visual streak area even after 7 months of untreated diabetes.

4.1. ERG responses in diabetic Meriones shawi

ERG is the most frequently used noninvasive measurement for the assessment of retinal function (Dorfman et al., 2014) and considered a sensitive marker of early neuronal abnormalities, long before DR can be clinically detected. Alterations in ERG responses have been detected in several animal models as well as in humans with diabetes (Dos Santos

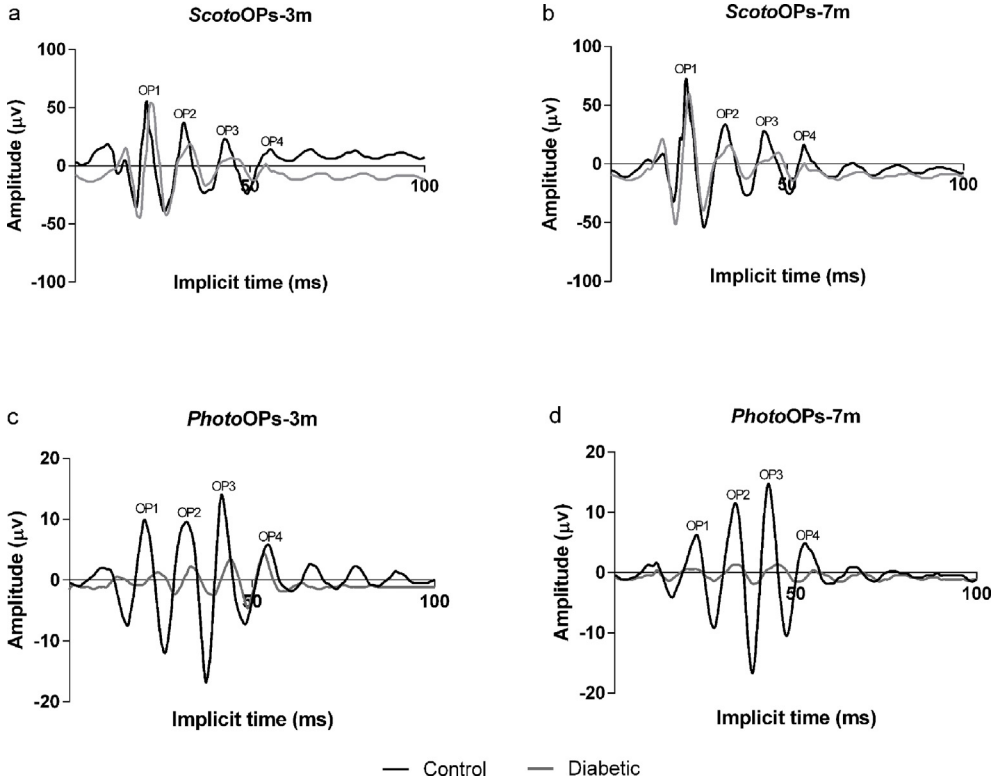

Fig. 3. Diabetes induces abnormal scotopic and photopic oscillatory potentials in *Meriones shawi*. Representative scotopic oscillatory potentials (*scoto*OPs) and photopic oscillatory potentials (*photo*OPs) extracted from 3 cd s m^{-2} mixed response and cone response respectively in control and diabetic *M.sh* at 3 months (3 m) (a-c) and 7 months (7 m) (b-d). A decrease in the amplitude of scotopic OP2, OP3, OP4 and ΣOPs was noticed after 3 and 7 months of diabetes. Significantly longer implicit times for scotopic OP2 and OP3 were detectable in both 3 and 7 months diabetic animals. A decrease in the amplitude of all the photopic OPs was noticed at both 3 and 7 months of diabetes. The implicit time for photopic OP1, OP2, OP3 was delayed after 3 months of diabetes while only OP3 and OP4 implicit times were altered in 7 months diabetic animals.

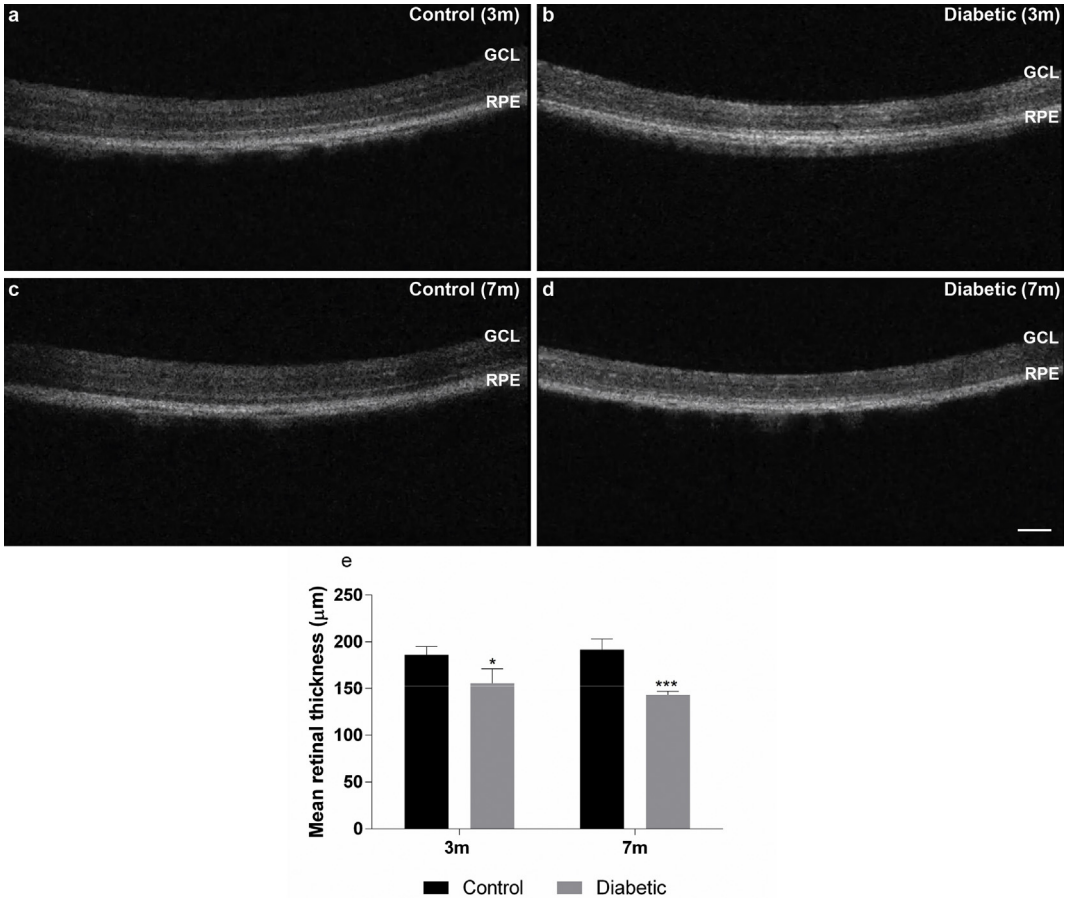

Fig. 4. Retinal layering and thickness analysis on OCT images in diabetic *Meriones shawi*. *In vivo* OCT images (a–e) showed a decrease in total retinal thickness measured from the nerve fiber layer to the outer segment layer in diabetic *M.sh* both after 3 months (3 m) and 7 months (7 m) of diabetes. GCL: ganglion cell layer, RPE: retinal pigment epithelium, *p < 0.05, ***p < 0.001, Bar: 100 µm.

et al., 2017; Fernandez et al., 2011; Kohzaki et al., 2008; Shinoda et al., 2007). In diabetic *M.sh* several ERG abnormalities were detectable, under scotopic and also under photopic conditions, suggesting that rod and cone pathways are both susceptible to diabetes. The results are similar to those found in another HFD-induced obesity mouse (Chang et al., 2015) and in other diabetic animal models as well as in human patients. The ERG alterations also show good correlation with the results of morphological changes detectable. The summary of ERG alterations and the proposed correlation between retinal dysfunction and morphological alterations in diabetic *Meriones shawi* is summarized in Table 3.

4.2. Scotopic and photopic photoreceptoral a-wave in diabetic Meriones shawi

The a-wave originates from rods and cones and reflects the functional stage of photoreceptors (Yune et al., 2007). In our animal model, a significant decrease in the amplitude of the scotopic and photopic a-wave was evident and a delayed latency was present in the photopic a-wave in 7 months diabetic animals. This is similar to what have been observed in several other diabetic animals (Li et al., 2002; Phipps et al., 2004, 2006) and in patients with type 1 diabetes even without clinical symptoms of DR (Juen and Kieselbach, 1990).The mechanisms for amplitude loss of a-wave may include the reduction in the number of rod photoreceptor outer segments (Breton et al., 1995). In line with these our previous experimental studies by immunohistochemistry (Hammoum et al., 2017a) showed rod and cone photoreceptor degeneration with a deterioration of outer segment morphology and significant loss in the number of total cones and M-cones in diabetic *M.sh* retinas showing that photoreceptors were indeed altered by the pathological processes of DR.

4.3. Scotopic and photopic b-wave in diabetic Meriones shawi

The b-wave mainly reflects the electrical activity of the inner nuclear layer (Yune et al., 2007). The dark-adapted b-wave is initiated by depolarization of the ON-bipolar cells, which induces potassium efflux from the Müller cell endfeet (Sieving et al., 1994). In our study, both dark- and light-adapted b-wave amplitude decreased and the implicit time of both scotopic and photopic b-wave was also delayed in diabetic animals at both time points. A comparative study done on streptozotocin-induced diabetes in Lewis, Wistar and Sprague Dawley rats (Kern et al., 2010) showed that in all strains diabetes induced the impairment of dark-adapted b-wave amplitude. The amplitude of the b-wave of the scotopic Ff-ERG is abnormal in diabetic patients even in the absence of clinical signs of DR (Coupland, 1987; Hardy et al., 1995). As a possible explanation, morphological findings in our previous studies (Hammoum et al., 2017a, 2017b) showed an increased expression of GFAP in Müller cells as a sign of glial activation and a decrease in the intensity of PKC-α labeling of rod bipolar cells in diabetic *M.sh* retina suggesting that Müller cell reactivity and rod bipolar cells alteration correlate well with functional alteration of the b-wave.

4.4. 30 Hz flicker response in diabetic Meriones shawi

Reductions in amplitude and delayed implicit time of 30-Hz flicker ERG have also been identified as a functional marker of DR, but they were associated with the more advanced stages of the disease (Chung

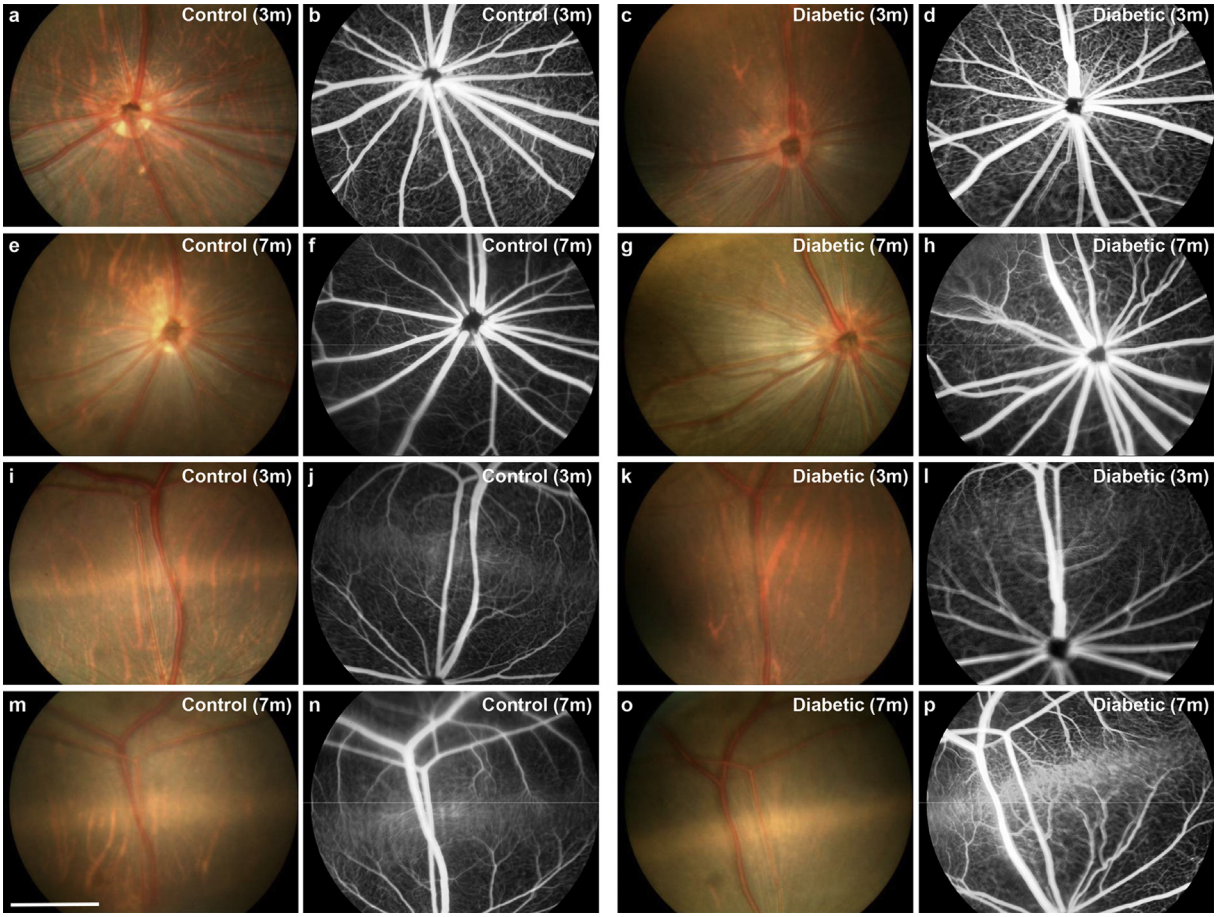

Fig. 5. Retinal vasculature analysis on eye fundus and fluorescein angiography images in *Meriones shawi*. Fundus images and fluorescein angiographs of retinal vasculature did not show any pattern of vascular abnormalities in the optic nerve (a–h) or in the visual streak (i–p) area neither after 3 months (3 m) nor after 7 months (7 m) of diabetes. Bar: 1 mm.

et al., 1993). It has also been shown that the implicit time of photopic 30-Hz flicker ERG is associated with the severity of DR (Bresnick and Palta, 1987b; Holopigian et al., 1992; Jansson et al., 2015). In *M.sh* we have detected a significant decrease in the amplitude of 30-Hz flicker ERG both after 3 and 7 months of diabetes but without any delay in the latency confirming one more time the major alteration of cone photoreceptors.

4.5. Scotopic and photopic inner retinal oscillatory potentials in diabetic Meriones shawi

Many publications have pointed out that the OPs are the most sensitive electrophysiologic indicators of DR (Hancock and Kraft, 2004; Holopigian et al., 2000; Juen and Kieselbach, 1990; Vadala et al., 2002). It has been suggested that OPs originate from amacrine cells and pharmacologic studies showed that dopamine (Wachtmeister and Dowling, 1978), γ-aminobutyric acid (GABA), and glycine blockers (Wachtmeister, 1980) all diminish the OPs. Many studies in diabetic rodents (Hancock and Kraft, 2004; Sakai et al., 1995) as well as in human patients (Gliem et al., 1971; Yonemura et al., 1962) have shown changes in OPs that suggest inner retinal dysfunction. In line with this, in our study, amplitudes of scotopic OPs of diabetic *M. sh* were significantly lower than controls. Additionally, we found a decrease in four photopic OPs in diabetic *M.sh* showing that both rod and cone pathways are altered in *M.sh* under diabetic conditions. Results of morphological examinations parallel with the detected alterations of the OPs. As far as amacrine cells are concerned, although our previous structural studies (Hammoum et al., 2017a) showed no change in dopaminergic and cholinergic amacrine cells, we noticed a decrease of the intensity of GAD 65&67 labeling in GABAergic amacrine cells under diabetic conditions. Also, a significant decrease in the number of amacrine cells labeled by different calcium binding proteins such the parvalbumin and calretinin was detectable.

4.6. Retinal thickness in diabetic Meriones shawi

Several clinical studies by OCT have shown the thinning of the retinal ganglion cell layer in diabetic patients with little or no symptoms of vascular retinopathy both in type 1 and type 2 diabetic patients (van Dijk et al., 2010, 2012). A decrease of approximately 5% was estimated in the early stages of DR. It was assumed to have a clinical consequence due to its correlation with the functional alterations detected (Biallosterski et al., 2007). Similarly, a significant reduction in the thickness by OCT was also noticed in diabetic *M.sh* which correlated well with our histological experiments (Hammoum et al., 2017a, 2017b). A significant decrease of retinal thickness was also found in other animal models, including leptin-deficient mice after 22 weeks (Zhi et al., 2014), OLETF rat (Yang et al., 2013) and Ins^{2Akita} mice after 3, 6 and 9 months of age (Hombrebueno et al., 2014).

4.7. Vascular alterations in diabetic Meriones shawi

Studies of vascular alterations have been carried out extensively on transgenic mice models. Although a series of microscopic vascular alterations have been described in diabetic mice (Huber et al., 2011; McLenachan et al., 2013), these models fail to reproduce the clinical

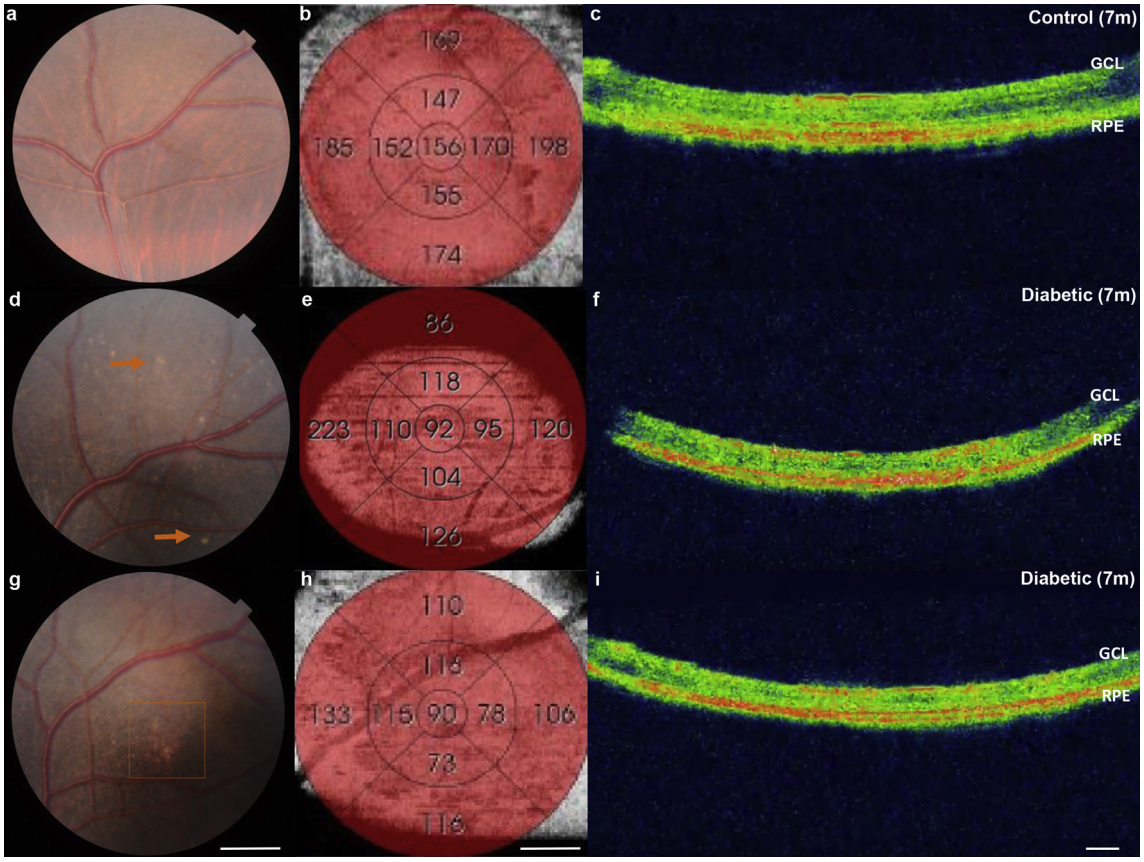

Fig. 6. Peripheral retinal alterations after 7 months of diabetes in *Meriones shawi*. Fundus (a, d, g – left column), OCT (c, f, I – right column) images and isodensity maps (b, e, h – middle column) from control (upper row) and diabetic *M.sh.* lower two rows. Diabetic specimens showed vascular abnormalities after 7 months of diabetes with the presence of exudates in the superior periphery (arrows and quadrangle). Isodensity maps (e, h) showed disproportional distribution of retinal thicknesses in the altered zones. GCL: ganglion cell layer, RPE: retinal pigment epithelium, Bar: 1 mm for left and middle columns and 100 μm for the right column.

symptoms that appear in the advanced stages of DR. A work performed on the SHR/N-cp rat, a spontaneously hypertensive animal model developing type 2 diabetes, showed the absence of detectable vascular alterations by fluorescein angiography and also the absence of all clinical signs such as exudates by ophthalmoscopy after 4 and 8 months of age (Huber et al., 2011). Similarly, no vascular changes were observed by fluorescein angiography in the Ins^{2Akita} mouse even after 25 weeks of age (McLenachan et al., 2013). In other animal models of diabetes, like in STZ-induced diabetic rats, the first clinically detectable vascular alterations (dilatation of venules and arterioles) appear only after 24 weeks (Kumar Gupta et al., 2013). Today therefore, exclusively VEGF overexpressing animals are used to model clinically detectable diabetic vascular alterations. Kimba mouse show retinal neovascularization after 3–4 weeks of age with hemorrhage, retinal detachment and microaneurysms (Rakoczy et al., 2010). Similarly, the presence of hemorrhages, decreased fluorescein in the capillaries and neovascularization has been shown in the Akimba mouse (Ali Rahman et al., 2011; Rakoczy et al., 2010; Wisniewska-Kruk et al., 2014). Not surprisingly therefore, in *M.sh*, no clinically detectable vascular symptoms where found after 3 months of diabetes neither in the periphery nor in the central retina.

Furthermore no sign of edema was detected in the visual streak area even after 7 months of untreated diabetes. This parallels previous morphologic findings (Hammoum et al., 2017b) and indicates that 7 months – the longest observation period used in this study – is not sufficient to develop macular pathology like alterations in this species. Further studies are on the way to examine if longer periods of diabetes will induce specific pathological alterations in the visual streak area as well. Some exudates however, were found in the superior peripheral retina of 7 months diabetic animals confirming that clinically detectable vascular alterations appear only at an advanced stage of DR well preceded by other structural and functional alterations.

4.8. Glutamate metabolism and presynaptic proteins in diabetic Meriones shawi

Several studies suggest that retinal glutamate metabolism may be compromised by diabetes, and could explain the glial reactivity, neuronal apoptosis and impairment of retinal function; key proteins of glutamate metabolism and their possible connection with functional alterations have not been studied previously in *M.sh*. Increased glutamate is found under pathological conditions in various neurological disorders and in neurodegenerative diseases including DR (Lau and Tymianski, 2010; Lewerenz and Maher, 2015; Lieth et al., 1998; Sheldon and Robinson, 2007). Excitotoxic neurodegeneration occurs due to the presence of glutamate excess in the synaptic space that may be the consequence of the defect in glutamate disposal pathways within Müller cells (Lieth et al., 1998, 2000). Diabetes reduces the ability of explant retinas to convert [14C] glutamate into [14C] glutamine, possibly because of a reduction in the content of the glial enzyme, glutamine synthetase (Lieth et al., 1998). Downregulation of GS was also reported here in diabetic *M.sh* both after 3 and 7 months of diabetes and similarly in diabetic *Psammomys obesus* after 7 months (Saidi et al., 2011a; 2011b). GS inhibition by using L-methionine sulfoximine leads to a reduction of the b-wave amplitude (Barnett et al., 2000; Bui et al., 2009). In addition, inhibition of glutamate uptake using

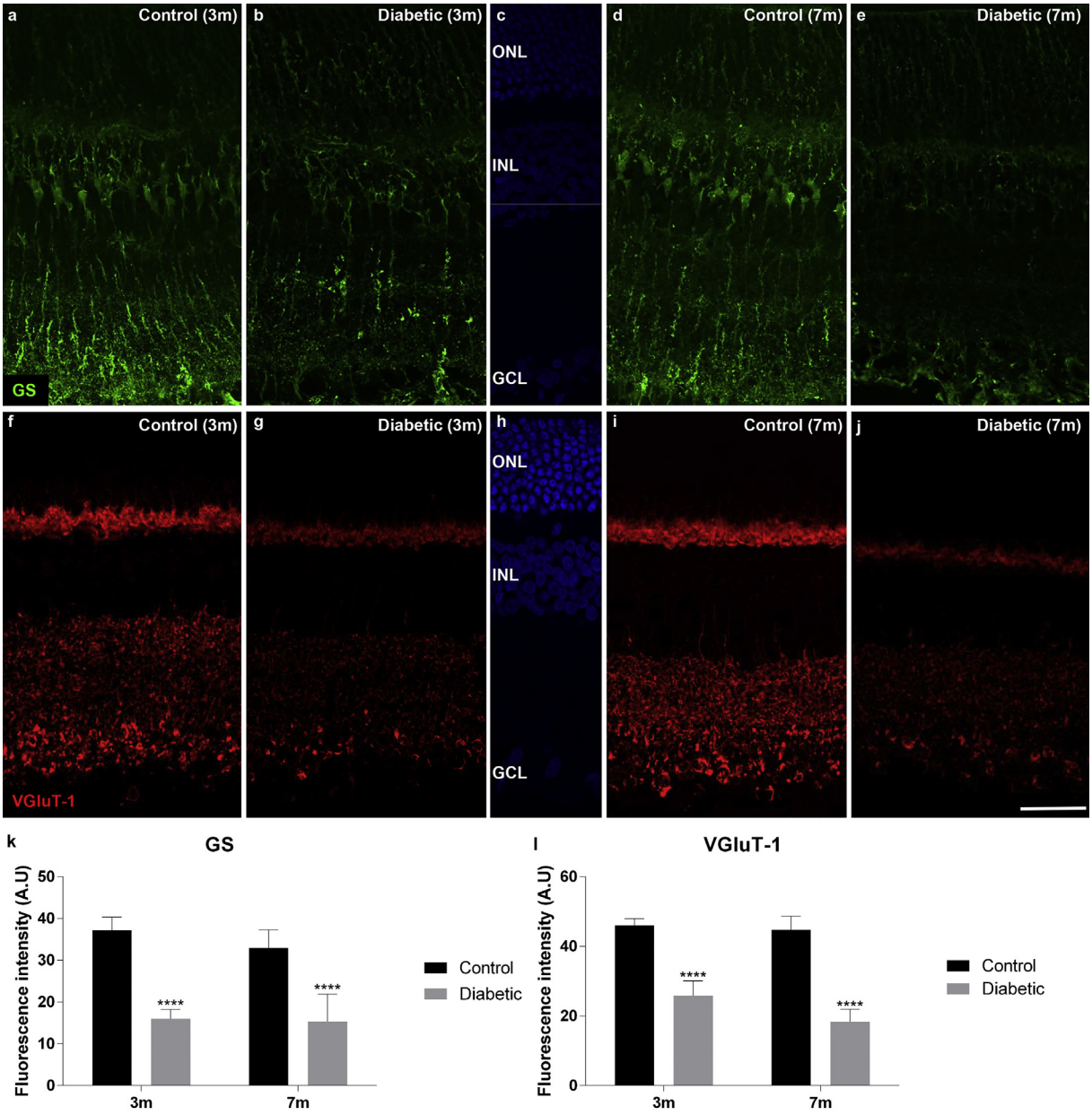

Fig. 7. Diabetes induces impairment in glutamate metabolism. Representative pictures of Müller cells labeled with glutamine synthetase (GS, a-e) and glutamatergic nerve terminals with vesicular glutamate transporter-1(VGluT-1, f-j) in control and diabetic retinas. GS expression was seen in Müller cells vertically throughout the retina in controls at 3 months (3 m, a) and at 7 months (7 m, d). A decrease of GS staining intensity was detected in diabetic animals after 3 and 7 months (b and e respectively) compared to age-matched controls. Quantifications revealed a significant decrease in staining intensity for both time points (k). A strong staining of VGluT-1 was seen in the plexiform layers in control animals (f, i). A decrease in the VGluT-1 expression was detected in diabetic animals (g, j) which again proved to be significant with quantification (l) both at 3 m and 7 m. DAPI staining is used to delineate retinal layers (c, h). ONL: outer nuclear layer, INL: inner nuclear layer, GCL: ganglion cell layer, A.U: arbitrary unit, ****p < 0,0001, Bar: 40 μm.

threohydroxyaspartic acid and D-aspartate (Winkler et al., 1999) selectively attenuates the depolarizing-bipolar cell dominated b-wave (Stockton and Slaughter, 1989). These results confirm once more the possible correlation between structure and function in *M.sh,* since a decrease of both GS expression and the amplitude of scotopic and photopic b-wave was reported.

VGluT1 is the major transporter responsible for loading glutamate into synaptic vesicles, and is expressed at ribbon synapses in photoreceptors in the outer plexiform layer and ON bipolar cells in the inner plexiform layer (Sherry et al., 2003). VGluT-1 was shown to be decreased in the retina of 10-week-old diabetic db/db mouse (Ly et al., 2014) and a significant decrease in the content of both VGLUT-1 and -2 was observed in retinal synaptosomes as early as after two weeks in streptozotocin induced diabetic rats (Baptista et al., 2011). These results are in agreement with our findings in diabetic *M. sh*, in which VGluT-1 expression was significantly decreased in diabetic retinas. This decrease in VGluT-1 might result in altered rates and amounts of glutamate loading, affecting the magnitude of signal transmission from photoreceptors to bipolar cells and between post-receptoral neurons (Ly et al., 2014).

Reduced synaptophysin content, a presynaptic protein, is also a recurrent finding in several studies on diabetic rats (D'Cruz et al., 2012; Duarte et al., 2009; Gaspar et al., 2010; Jiang et al., 2010; Kurihara et al., 2008; Sasaki et al., 2010). Similarly, a decrease in synaptophysin expression was detected in diabetic *M.sh* which correlates with abnormal ERG retinal responses noticed in diabetic animals. Many

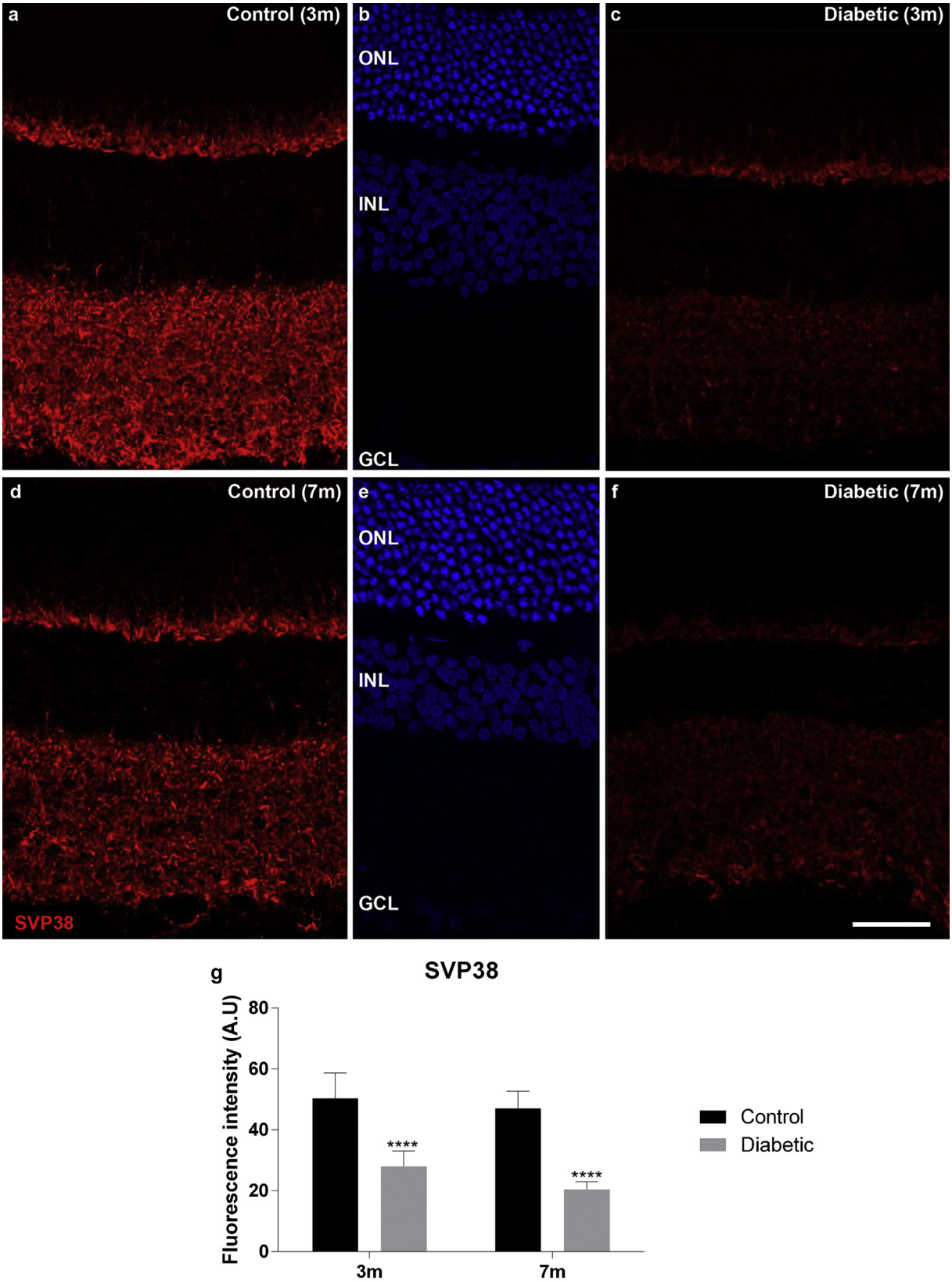

Fig. 8. Diabetes induces changes in presynaptic protein expression. Representative pictures of synaptic terminals labeled with synpatophysin protein 38 KDa (SVP38) in control (a, d) and diabetic retinas (c, f). SVP38 expression was intense in the plexiform layers in 3 months (3 m) and 7 months (7 m) control animals. Diabetes induced a decrease in the SVP38 staining both in 3 and 7 months diabetic animals. Quantification for the IPL revealed significant differences in staining intensities at both time points (g). DAPI staining is used for orientation (b, e). ONL: outer nuclear layer, INL: inner nuclear layer, GCL: ganglion cell layer, A.U: arbitrary unit, ****p < 0,0001, Bar: 40 μm.

Table 3
Correlation between functional alterations and morphological findings in diabetic Meriones shawi.

ERG waves	Origin	Functional Alteration	Correlation with morphological findings	References
Scotopic and photopic a-wave	Rods and cones (hyperpolarization of rods and cones)	Amplitude decrease and delay in the implicit time	Rod and cone photoreceptor degeneration with a deterioration of outer segment morphology and significant loss in the number of total cones and M-cones	(Breton et al., 1995; Dellaa et al., 2018; Hammoum et al., 2017a; Juen and Kieselbach, 1990; Kim et al., 2017; Li et al., 2002; Phipps et al., 2004, 2006; Yune et al., 2007)
Scotopic and photopic b-wave	Bipolar cells and Müller cells (depolarization of the ON-bipolar cells which induces potassium efflux from the Müller cell endfeet)	Amplitude decrease and delay in the implicit time	Increased expression of GFAP in Müller cells as a sign of glial activation. Decrease in GS staining in Müller cells. Decrease in the intensity of PKC-α labeling of rod bipolar cells	(Coupland, 1987; Dellaa et al., 2018; Hammoum et al., 2017a, 2017b; Kim et al., 2017; Kern et al., 2010; Sieving et al., 1994; Yune et al., 2007)
Flicker response 30Hz	M-cone bipolar cells (depolarization of ON- cone bipolar cells)	Amplitude decrease	Cone photoreceptors alteration	(Bresnick and Palta, 1987b; Chung et al., 1993; Holopigian et al., 1992; Jansson et al., 2015)
Scotopic and photopic oscillatory potentials	Amacrine cells	Amplitude decrease and delay in the implicit time	A decrease of the intensity of GAD 65&67 labeling in GABAergic amacrine cells. A significant decrease in the number of amacrine cells labeled by different calcium binding proteins such the parvalbumin and calretinin was detectable.	(Gliem et al., 1971; Hammoum et al., 2017a; Hancock and Kraft, 2004; Holopigian et al., 2000; Juen and Kieselbach, 1990; Kohzaki et al., 2008; Sakai et al., 1995; Vadala et al., 2002; Wachtmeister, 1980; Wachtmeister and Dowling, 1978; Yonemura et al., 1962)

publications showed that a loss of synaptophysin might disrupt photoreceptor synapse and neurotransmitter release, significantly affecting retinal function (Singleton et al., 1997; Spiwoks-Becker et al., 2001; Stenius et al., 1995).

Overall the detected changes in glutamate metabolism and synaptophysin immunoreactivity correlate well with the detected functional alterations.

5. Conclusion

The present results show a remarkable retinal dysfunction induced by diabetes in *M.sh* with evidence that the disease alters both the rod and the cone pathways early. Results suggest that the function of the photoreceptors, represented by the a-wave, was more severely affected by diabetic conditions. Furthermore, functional results show high correlation with the results of retinal histological studies conducted here and previously (Hammoum et al., 2017a, 2017b). We confirmed also in *M.sh* that neurodegeneration and retinal dysfunction occur before the clinically detectable vascular alterations would be present. Hence, the necessity of the early detection of the early changes in DR such as retinal structural and functional alterations that may help for preventing vision loss.

Conflicts of interest

The authors declare no conflicts of interest.

Acknowledgements

Special thanks to Anna Énzsöly for the valuable advices throughout the preparation of the manuscript. We thank the Ministry of Tunisian Agriculture (Forest direction) for their authorization to experiment on animals and their help to capture animals.

Financial support: This research is performed in the framework of MOBIDOC launched under the Support Project to the Research and Innovation System (PASRI) funded by the European Union (EU) and managed by the National Agency for the Promotion of Scientific Research (ANPR) in partnership with UNIMED Laboratories.

References

Aissaoui, A., Zizi, S., Israili, Z.H., Lyoussi, B., 2011. Hypoglycemic and hypolipidemic effects of Coriandrum sativum L. in Meriones shawi rats. J. Ethnopharmacol. 137 (1), 652–661. https://doi.org/10.1016/j.jep.2011.06.019.

Ali Rahman, I.S., Li, C.R., Lai, C.M., Rakoczy, E.P., 2011. In vivo monitoring of VEGF-induced retinal damage in the Kimba mouse model of retinal neovascularization. Curr. Eye Res. 36 (7), 654–662. https://doi.org/10.3109/02713683.2010. 551172.

Baptista, F.I., Gaspar, J.M., Cristovao, A., Santos, P.F., Kofalvi, A., Ambrosio, A.F., 2011. Diabetes induces early transient changes in the content of vesicular transporters and no major effects in neurotransmitter release in hippocampus and retina. Brain Res. 1383, 257–269. https://doi.org/10.1016/j.brainres.2011.01.071.

Barber, A.J., Antonetti, D.A., Gardner, T.W., 2000. Altered expression of retinal occludin and glial fibrillary acidic protein in experimental diabetes. The Penn State Retina Research Group. Invest. Ophthalmol. Vis. Sci. 41 (11), 3561–3568.

Barber, A.J., Lieth, E., Khin, S.A., Antonetti, D.A., Buchanan, A.G., Gardner, T.W., 1998. Neural apoptosis in the retina during experimental and human diabetes. Early onset and effect of insulin. J. Clin. Invest. 102 (4), 783–791. https://doi.org/10.1172/JCI2425.

Barnett, N.L., Pow, D.V., Robinson, S.R., 2000. Inhibition of Muller cell glutamine synthetase rapidly impairs the retinal response to light. Glia 30 (1), 64–73.

Biallosterski, C., van Velthoven, M.E., Michels, R.P., Schlingemann, R.O., DeVries, J.H., Verbraak, F.D., 2007. Decreased optical coherence tomography-measured pericentral retinal thickness in patients with diabetes mellitus type 1 with minimal diabetic retinopathy. Br. J. Ophthalmol. 91 (9), 1135–1138. https://doi.org/10.1136/bjo.2006.111534.

Bresnick, G.H., Palta, M., 1987. Temporal aspects of the electroretinogram in diabetic retinopathy. Arch. Ophthalmol. 105 (5), 660–664.

Breton, M.E., Quinn, G.E., Schueller, A.W., 1995. Development of electroretinogram and rod phototransduction response in human infants. Invest. Ophthalmol. Vis. Sci. 36 (8), 1588–1602.

Bui, B.V., Hu, R.G., Acosta, M.L., Donaldson, P., Vingrys, A.J., Kalloniatis, M., 2009. Glutamate metabolic pathways and retinal function. J. Neurochem. 111 (2), 589–599. https://doi.org/10.1111/j.1471-4159.2009.06354.x.

Chang, R.C., Shi, L., Huang, C.C., Kim, A.J., Ko, M.L., Zhou, B., Ko, G.Y., 2015. High-fat diet-induced retinal dysfunction. Invest. Ophthalmol. Vis. Sci. 56 (4), 2367–2380. https://doi.org/10.1167/iovs.14-16143.

Chung, N.H., Kim, S.H., Kwak, M.S., 1993. The electroretinogram sensitivity in patients with diabetes. Korean J. Ophthalmol. Times. 7 (2), 43–47.

Congdon, N.G., Friedman, D.S., Lietman, T., 2003. Important causes of visual impairment in the world today. J. Am. Med. Assoc. 290 (15), 2057–2060. https://doi.org/10.1001/jama.290.15.2057.

Coupland, S.G., 1987. A comparison of oscillatory potential and pattern electroretinogram measures in diabetic retinopathy. Doc. Ophthalmol. Times. 66 (3), 207–218.

Dan, C., Jian-Bin, T., Hui, W., Le-Ping, Z., Jin, Z., Ju-Fang, H., Xue-Gang, L., 2008. Synaptophysin expression in rat retina following acute high intraocular pressure. Acta Histochem. Cytochem. 41 (6), 173–178. https://doi.org/10.1267/ahc.08034.

D'Cruz, T.S., Weibley, B.N., Kimball, S.R., Barber, A.J., 2012. Post-translational processing of synaptophysin in the rat retina is disrupted by diabetes. PLoS One 7 (9), e44711. https://doi.org/10.1371/journal.pone.0044711.

Dellaa, A., Benlarbi, M., Hammoum, I., Gammoudi, N., Dogui, M., Messaoud, R., Azaiz, R., Charfeddine, R., Khairallah, M., Lachapelle, P., Ben Chaouacha-Chekir, R., 2018. Electroretinographic evidence suggesting that the type 2 diabetic retinopathy of the sand rat Psammomys obesus is comparable to that of humans. PloS one 13, e0192400.

Dellaa, A., Polosa, A., Mbarek, S., Hammoum, I., Messaoud, R., Amara, S., Azaiz, R., Charfeddine, R., Dogui, M., Khairallah, M., Lachapelle, P., Ben Chaouacha-Chekir, R., 2016. Characterizing the retinal function of Psammomys obesus: a diurnal rodent model to study human retinal function. Curr. Eye Res. 1–9. https://doi.org/10.3109/02713683.2016.1141963.

Dorfman, D., Aranda, M.L., Gonzalez Fleitas, M.F., Chianelli, M.S., Fernandez, D.C., Sande, P.H., Rosenstein, R.E., 2014. Environmental enrichment protects the retina from early diabetic damage in adult rats. PloS One 9, e101829.

Duarte, J.M., Carvalho, R.A., Cunha, R.A., Gruetter, R., 2009. Caffeine consumption attenuates neurochemical modifications in the hippocampus of streptozotocin-induced diabetic rats. J. Neurochem. 111 (2), 368–379. https://doi.org/10.1111/j.1471-4159.2009.06349.x.

Fernandez, D.C., Sande, P.H., Chianelli, M.S., Aldana Marcos, H.J., Rosenstein, R.E., 2011. Induction of ischemic tolerance protects the retina from diabetic retinopathy. Am. J. Pathol. 178 (5), 2264–2274. https://doi.org/10.1016/j.ajpath.2011.01.040.

Gardner, T.W., Antonetti, D.A., Barber, A.J., LaNoue, K.F., Levison, S.W., 2002. Diabetic retinopathy: more than meets the eye. Surv. Ophthalmol. 47 (Suppl. 2), S253–S262.

Gaspar, J.M., Castilho, A., Baptista, F.I., Liberal, J., Ambrosio, A.F., 2010. Long-term exposure to high glucose induces changes in the content and distribution of some exocytotic proteins in cultured hippocampal neurons. Neuroscience 171 (4), 981–992. https://doi.org/10.1016/j.neuroscience.2010.10.019.

Ghirlanda, G., Di Leo, M.A., Caputo, S., Cercone, S., Greco, A.V., 1997. From functional to microvascular abnormalities in early diabetic retinopathy. Diabetes Metab. Rev. 13 (1), 15–35.

Gliem, H., Moller, D.E., Kietzmann, G., 1971. The bioelectric activity of the retina in diabetic retinopathy. Acta Ophthalmol. 49 (3), 353–363.

Greenstein, V., Sarter, B., Hood, D., Noble, K., Carr, R., 1990. Hue discrimination and S cone pathway sensitivity in early diabetic retinopathy. Invest. Ophthalmol. Vis. Sci. 31 (6), 1008–1014.

Hammoum, I., Benlarbi, M., Dellaa, A., Szabo, K., Dekany, B., Csaba, D., Almasi, Z., Hajdu, R.I., Azaiz, R., Charfeddine, R., Lukats, A., Ben Chaouacha-Chekir, R., 2017a. Study of retinal neurodegeneration and maculopathy in diabetic Meriones shawi: a particular animal model with human-like macula. J. Comp. Neurol. 525, 2890–2914. https://doi.org/10.1002/cne.24245.

Hammoum, I., Mbarek, S., Dellaa, A., Dubus, E., Baccouche, B., Azaiz, R., Charfeddine, R., Picaud, S., Ben Chaouacha-Chekir, R., 2017b. Study of retinal alterations in a high fat diet-induced type ii diabetes rodent: Meriones shawi. Acta Histochem. 119 (1), 1–9. https://doi.org/10.1016/j.acthis.2016.05.005.

Hancock, H.A., Kraft, T.W., 2004. Oscillatory potential analysis and ERGs of normal and diabetic rats. Invest. Ophthalmol. Vis. Sci. 45 (3), 1002–1008.

Hardy, K.J., Fisher, C., Heath, P., Foster, D.H., Scarpello, J.H., 1995. Comparison of colour discrimination and electroretinography in evaluation of visual pathway dysfunction in aretinopathic IDDM patients. Br. J. Ophthalmol. 79 (1), 35–37.

Hardy, K.J., Lipton, J., Scase, M.O., Foster, D.H., Scarpello, J.H., 1992. Detection of colour vision abnormalities in uncomplicated type 1 diabetic patients with angiographically normal retinas. Br. J. Ophthalmol. 76 (8), 461–464.

Holopigian, K., Greenstein, V.C., Seiple, W., Hood, D.C., Ritch, R., 2000. Electrophysiologic assessment of photoreceptor function in patients with primary open-angle glaucoma. J. Glaucoma 9 (2), 163–168.

Holopigian, K., Seiple, W., Lorenzo, M., Carr, R., 1992. A comparison of photopic and scotopic electroretinographic changes in early diabetic retinopathy. Invest. Ophthalmol. Vis. Sci. 33 (10), 2773–2780.

Hombrebueno, J.R., Chen, M., Penalva, R.G., Xu, H., 2014. Loss of synaptic connectivity, particularly in second order neurons is a key feature of diabetic retinal neuropathy in the Ins2Akita mouse. PLoS One 9 (5), e97970. https://doi.org/10.1371/journal.pone.0097970.

Huber, G., Heynen, S., Imsand, C., vom Hagen, F., Muehlfriedel, R., Tanimoto, N., Feng, Y., Hammes, H.P., Grimm, C., Peichl, L., Seeliger, M.W., Beck, S.C., 2010. Novel rodent models for macular research. PLoS One 5 (10), e13403. https://doi.org/10.1371/journal.pone.0013403.

Huber, M., Heiduschka, P., Ziemssen, F., Bolbrinker, J., Kreutz, R., 2011. Microangiopathy and visual deficits characterize the retinopathy of a spontaneously hypertensive rat model with type 2 diabetes and metabolic syndrome. Hypertens. Res. 34 (1), 103–112. https://doi.org/10.1038/hr.2010.168.

Jackson, G.R., Barber, A.J., 2010. Visual dysfunction associated with diabetic retinopathy. Curr. Diabetes Rep. 10 (5), 380–384. https://doi.org/10.1007/s11892-010-0132-4.

Jansson, R.W., Raeder, M.B., Krohn, J., 2015. Photopic full-field electroretinography and optical coherence tomography in type 1 diabetic retinopathy. Graefes Arch. Clin. Exp. Ophthalmol. 253 (7), 989–997. https://doi.org/10.1007/s00417-015-3034-y.

Jiang, Y., Walker, R.J., Kern, T.S., Steinle, J.J., 2010. Application of isoproterenol inhibits diabetic-like changes in the rat retina. Exp. Eye Res. 91 (2), 171–179. https://doi.org/10.1016/j.exer.2010.04.014.

Johnson, J., Tian, N., Caywood, M.S., Reimer, R.J., Edwards, R.H., Copenhagen, D.R., 2003. Vesicular neurotransmitter transporter expression in developing postnatal rodent retina: GABA and glycine precede glutamate. J. Neurosci. 23 (2), 518–529.

Juen, S., Kieselbach, G.F., 1990. Electrophysiological changes in juvenile diabetics without retinopathy. Arch. Ophthalmol. 108 (3), 372–375.

Kern, T.S., Miller, C.M., Tang, J., Du, Y., Ball, S.L., Berti-Matera, L., 2010. Comparison of three strains of diabetic rats with respect to the rate at which retinopathy and tactile allodynia develop. Mol. Vis. 16, 1629–1639.

Kim, A.J., Chang, J.Y., Shi, L., Chang, R.C., Ko, M.L., Ko, G.Y., 2017. The effects of metformin on obesity-induced dysfunctional retinas. IOVS (Investig. Ophthalmol. Vis. Sci.) 58, 106–118.

Klein, B.E., 2007. Overview of epidemiologic studies of diabetic retinopathy. Ophthalmic Epidemiol. 14 (4), 179–183. https://doi.org/10.1080/09286580701396720.

Kohzaki, K., Vingrys, A.J., Bui, B.V., 2008. Early inner retinal dysfunction in streptozotocin-induced diabetic rats. Invest. Ophthalmol. Vis. Sci. 49 (8), 3595–3604. https://doi.org/10.1167/iovs.08-1679.

Kumar Gupta, S., Kumar, B., Srinivasan, B.P., Nag, T.C., Srivastava, S., Saxena, R., Aggarwal, A., 2013. Retinoprotective effects of Moringa oleifera via antioxidant, anti-inflammatory, and anti-angiogenic mechanisms in streptozotocin-induced diabetic rats. J. Ocul. Pharmacol. Ther. 29, 419–426.

Kurihara, T., Ozawa, Y., Nagai, N., Shinoda, K., Noda, K., Imamura, Y., Tsubota, K., Okano, H., Oike, Y., Ishida, S., 2008. Angiotensin II type 1 receptor signaling contributes to synaptophysin degradation and neuronal dysfunction in the diabetic retina. Diabetes 57 (8), 2191–2198. https://doi.org/10.2337/db07-1281.

Lai, A.K., Lo, A.C., 2013. Animal models of diabetic retinopathy: summary and comparison. J. Diabetes Res. 2013, 106594. https://doi.org/10.1155/2013/106594.

Lau, A., Tymianski, M., 2010. Glutamate receptors, neurotoxicity and neurodegeneration. Pflügers Archiv 460 (2), 525–542. https://doi.org/10.1007/s00424-010-0809-1.

Lewerenz, J., Maher, P., 2015. Chronic glutamate toxicity in neurodegenerative diseases-what is the evidence? Front. Neurosci. 9, 469. https://doi.org/10.3389/fnins.2015.00469.

Li, Q., Zemel, E., Miller, B., Perlman, I., 2002. Early retinal damage in experimental diabetes: electroretinographical and morphological observations. Exp. Eye Res. 74 (5), 615–625. https://doi.org/10.1006/exer.2002.1170.

Lieth, E., Barber, A.J., Xu, B., Dice, C., Ratz, M.J., Tanase, D., Strother, J.M., 1998. Glial reactivity and impaired glutamate metabolism in short-term experimental diabetic retinopathy. Penn State Retina Research Group. Diabetes 47 (5), 815–820.

Lieth, E., LaNoue, K.F., Antonetti, D.A., Ratz, M., 2000. Diabetes reduces glutamate oxidation and glutamine synthesis in the retina. The Penn State Retina Research Group. Exp. Eye Res. 70 (6), 723–730. https://doi.org/10.1006/exer.2000.0840.

Ly, A., Scheerer, M.F., Zukunft, S., Muschet, C., Merl, J., Adamski, J., de Angelis, M.H., Neschen, S., Hauck, S.M., Ueffing, M., 2014. Retinal proteome alterations in a mouse model of type 2 diabetes. Diabetologia 57 (1), 192–203. https://doi.org/10.1007/s00125-013-3070-2.

Marmor, M.F., Holder, G.E., Seeliger, M.W., Yamamoto, S., International Society for Clinical Electrophysiology of, V, 2004. Standard for clinical electroretinography (2004 update). Doc. Ophthalmol. 108 (2), 107–114.

McLenachan, S., Chen, X., McMenamin, P.G., Rakoczy, E.P., 2013. Absence of clinical correlates of diabetic retinopathy in the Ins2Akita retina. Clin. Exp. Ophthalmol. 41 (6), 582–592. https://doi.org/10.1111/ceo.12084.

Nag, T.C., Wadhwa, S., 2001. Differential expression of syntaxin-1 and synaptophysin in the developing and adult human retina. J. Biosci. 26 (2), 179–191.

Nguyen, T.T., Wang, J.J., Wong, T.Y., 2007. Retinal vascular changes in pre-diabetes and prehypertension: new findings and their research and clinical implications. Diabetes Care 30 (10), 2708–2715. https://doi.org/10.2337/dc07-0732.

Paques, M., Guyomard, J.L., Simonutti, M., Roux, M.J., Picaud, S., Legargasson, J.F., Sahel, J.A., 2007. Panretinal, high-resolution color photography of the mouse fundus. Invest. Ophthalmol. Vis. Sci. 48 (6), 2769–2774. https://doi.org/10.1167/iovs.06-1099.

Phipps, J.A., Fletcher, E.L., Vingrys, A.J., 2004. Paired-flash identification of rod and cone dysfunction in the diabetic rat. Invest. Ophthalmol. Vis. Sci. 45 (12), 4592–4600. https://doi.org/10.1167/iovs.04-0842.

Phipps, J.A., Yee, P., Fletcher, E.L., Vingrys, A.J., 2006. Rod photoreceptor dysfunction in diabetes: activation, deactivation, and dark adaptation. Invest. Ophthalmol. Vis. Sci. 47 (7), 3187–3194. https://doi.org/10.1167/iovs.05-1493.

Rakoczy, E.P., Ali Rahman, I.S., Binz, N., Li, C.R., Vagaja, N.N., de Pinho, M., Lai, C.M., 2010. Characterization of a mouse model of hyperglycemia and retinal neovascularization. Am. J. Pathol. 177 (5), 2659–2670. https://doi.org/10.2353/ajpath.2010.090883.

Riepe, R.E., Norenburg, M.D., 1977. Muller cell localisation of glutamine synthetase in rat retina. Nature 268 (5621), 654–655.

Saidi, T., Mbarek, S., Chaouacha-Chekir, R.B., Hicks, D., 2011a. Diurnal rodents as animal models of human central vision: characterisation of the retina of the sand rat Psammomys obsesus. Graefes Arch. Clin. Exp. Ophthalmol. 249 (7), 1029–1037. https://doi.org/10.1007/s00417-011-1641-9.

Saidi, T., Mbarek, S., Omri, S., Behar-Cohen, F., Chaouacha-Chekir, R.B., Hicks, D., 2011b. The sand rat, Psammomys obesus, develops type 2 diabetic retinopathy

similar to humans. Invest. Ophthalmol. Vis. Sci. 52 (12), 8993–9004. https://doi.org/10.1167/iovs.11-8423.
Sakai, H., Tani, Y., Shirasawa, E., Shirao, Y., Kawasaki, K., 1995. Development of electroretinographic alterations in streptozotocin-induced diabetes in rats. Ophthalmic Res. 27 (1), 57–63.
Salz, D.A., Witkin, A.J., 2015. Imaging in diabetic retinopathy. Middle East Afr. J. Ophthalmol 22 (2), 145–150. https://doi.org/10.4103/0974-9233.151887.
Santos, A.R., Ribeiro, L., Bandello, F., Lattanzio, R., Egan, C., Frydkjaer-Olsen, U., European Consortium for the Early Treatment of Diabetic, R, 2017. Functional and structural findings of neurodegeneration in early stages of diabetic retinopathy: cross-sectional analyses of baseline data of the EUROCONDOR Project. Diabetes 66 (9), 2503–2510. https://doi.org/10.2337/db16-1453.
Sasaki, M., Ozawa, Y., Kurihara, T., Kubota, S., Yuki, K., Noda, K., Kobayashi, S., Ishida, S., Tsubota, K., 2010. Neurodegenerative influence of oxidative stress in the retina of a murine model of diabetes. Diabetologia 53 (5), 971–979. https://doi.org/10.1007/s00125-009-1655-6.
Schindelin, J., Arganda-Carreras, I., Frise, E., Kaynig, V., Longair, M., Pietzsch, T., Cardona, A., 2012. Fiji: an open-source platform for biological-image analysis. Nat. Methods 9 (7), 676–682. https://doi.org/10.1038/nmeth.2019.
Sheldon, A.L., Robinson, M.B., 2007. The role of glutamate transporters in neurodegenerative diseases and potential opportunities for intervention. Neurochem. Int. 51 (6–7), 333–355. https://doi.org/10.1016/j.neuint.2007.03.012.
Sherry, D.M., Wang, M.M., Bates, J., Frishman, L.J., 2003. Expression of vesicular glutamate transporter 1 in the mouse retina reveals temporal ordering in development of rod vs. cone and ON vs. OFF circuits. J. Comp. Neurol. 465 (4), 480–498. https://doi.org/10.1002/cne.10838.
Shinoda, K., Rejdak, R., Schuettauf, F., Blatsios, G., Volker, M., Tanimoto, N., Olcay, T., Gekeler, F., Lehaci, C., Naskar, R., Zagorski, Z., Zrenner, E., 2007. Early electroretinographic features of streptozotocin-induced diabetic retinopathy. Clin. Exp. Ophthalmol. 35 (9), 847–854. https://doi.org/10.1111/j.1442-9071.2007.01607.x.
Sieving, P.A., Murayama, K., Naarendorp, F., 1994. Push-pull model of the primate photopic electroretinogram: a role for hyperpolarizing neurons in shaping the b-wave. Vis. Neurosci. 11 (3), 519–532.
Singleton, D.R., Wu, T.T., Castle, J.D., 1997. Three mammalian SCAMPs (secretory Carrier membrane proteins) are highly related products of distinct genes having similar subcellular distributions. J. Cell Sci. 110 (Pt 17), 2099–2107.
Spiwoks-Becker, I., Vollrath, L., Seeliger, M.W., Jaissle, G., Eshkind, L.G., Leube, R.E., 2001. Synaptic vesicle alterations in rod photoreceptors of synaptophysin-deficient mice. Neuroscience 107 (1), 127–142.
Stenius, K., Janz, R., Sudhof, T.C., Jahn, R., 1995. Structure of synaptogyrin (p29) defines novel synaptic vesicle protein. J. Cell Biol. 131 (6 Pt 2), 1801–1809.
Stockton, R.A., Slaughter, M.M., 1989. B-wave of the electroretinogram. A reflection of ON bipolar cell activity. J. Gen. Physiol. 93 (1), 101–122.
Vadala, M., Anastasi, M., Lodato, G., Cillino, S., 2002. Electroretinographic oscillatory potentials in insulin-dependent diabetes patients: a long-term follow-up. Acta Ophthalmol. Scandia. 80 (3), 305–309.
van Dijk, H.W., Verbraak, F.D., Kok, P.H., Garvin, M.K., Sonka, M., Lee, K., Devries, J.H., Michels, R.P., van Velthoven, M.E., Schlingemann, R.O., Abramoff, M.D., 2010. Decreased retinal ganglion cell layer thickness in patients with type 1 diabetes. Invest. Ophthalmol. Vis. Sci. 51 (7), 3660–3665. https://doi.org/10.1167/iovs.09-5041.
van Dijk, H.W., Verbraak, F.D., Kok, P.H., Stehouwer, M., Garvin, M.K., Sonka, M., DeVries, J.H., Schlingemann, R.O., Abramoff, M.D., 2012. Early neurodegeneration in the retina of type 2 diabetic patients. Invest. Ophthalmol. Vis. Sci. 53 (6), 2715–2719. https://doi.org/10.1167/iovs.11-8997.
Wachtmeister, L., 1980. Further studies of the chemical sensitivity of the oscillatory potentials of the electroretinogram (ERG) I. GABA- and glycine antagonists. Acta Ophthalmol. 58 (5), 712–725.
Wachtmeister, L., Dowling, J.E., 1978. The oscillatory potentials of the mudpuppy retina. Invest. Ophthalmol. Vis. Sci. 17 (12), 1176–1188.
Wang, B., Chandrasekera, P.C., Pippin, J.J., 2014. Leptin- and leptin receptor-deficient rodent models: relevance for human type 2 diabetes. Curr. Diabetes Rev. 10 (2), 131–145.
Winkler, B.S., Kapousta-Bruneau, N., Arnold, M.J., Green, D.G., 1999. Effects of inhibiting glutamine synthetase and blocking glutamate uptake on b-wave generation in the isolated rat retina. Vis. Neurosci. 16 (2), 345–353.
Wisniewska-Kruk, J., Klaassen, I., Vogels, I.M., Magno, A.L., Lai, C.M., Van Noorden, C.J., Schlingemann, R.O., Rakoczy, E.P., 2014. Molecular analysis of blood-retinal barrier loss in the Akimba mouse, a model of advanced diabetic retinopathy. Exp. Eye Res. 122, 123–131. https://doi.org/10.1016/j.exer.2014.03.005.
Xu, H., Koch, P., Chen, M., Lau, A., Reid, D.M., Forrester, J.V., 2008. A clinical grading system for retinal inflammation in the chronic model of experimental autoimmune uveoretinitis using digital fundus images. Exp. Eye Res. 87 (4), 319–326. https://doi.org/10.1016/j.exer.2008.06.012.
Yang, J.H., Kwak, H.W., Kim, T.G., Han, J., Moon, S.W., Yu, S.Y., 2013. Retinal neurodegeneration in type II diabetic otsuka long-evans tokushima fatty rats. Invest. Ophthalmol. Vis. Sci. 54 (6), 3844–3851. https://doi.org/10.1167/iovs.12-11309.
Yonemura, D., Aoki, T., Tsuzuki, K., 1962. Electroretinogram in diabetic retinopathy. Arch. Ophthalmol. 68, 19–24.
Yoshida, A., Kojima, M., Ogasawara, H., Ishiko, S., 1991. Oscillatory potentials and permeability of the blood-retinal barrier in noninsulin-dependent diabetic patients without retinopathy. Ophthalmology 98 (8), 1266–1271.
Yune, T.Y., Lee, J.Y., Jung, G.Y., Kim, S.J., Jiang, M.H., Kim, Y.C., Oh, Y.J., Markelonis, G.J., Oh, T.H., 2007. Minocycline alleviates death of oligodendrocytes by inhibiting pro-nerve growth factor production in microglia after spinal cord injury. J. Neurosci. 27 (29), 7751–7761. https://doi.org/10.1523/JNEUROSCI.1661-07.2007.
Zhang, B., Qiu, Q., Yin, L., Yao, Y., Wang, C., Wu, X., 2014. Measurement of retinal function with flash-electroretinography in Chinese patients with hyperlipidemia. Graefes Arch. Clin. Exp. Ophthalmol. 252 (9), 1385–1392. https://doi.org/10.1007/s00417-014-2726-z.
Zhi, Z., Chao, J.R., Wietecha, T., Hudkins, K.L., Alpers, C.E., Wang, R.K., 2014. Noninvasive imaging of retinal morphology and microvasculature in obese mice using optical coherence tomography and optical microangiography. Invest. Ophthalmol. Vis. Sci. 55 (2), 1024–1030. https://doi.org/10.1167/iovs.13-12864.